Mutational and pH Analysis of Ionic Residues in Transmembrane Domains of Vesicular Acetylcholine Transporter†

Dawn T. Bravo, Natalia G. Kolmakova, and Stanley M. Parsons*

Department of Chemistry and Biochemistry, University of California, Santa Barbara, California 93106

Received December 6, 2004; Revised Manuscript Received April 2, 2005

ABSTRACT: This research investigated the roles of 7 conserved ionic residues in the 12 putative transmembrane domains (TMDs) of vesicular acetylcholine transporter (VAChT). Rat VAChT in wild-type and mutant forms was expressed in PC12$^{A123.7}$ cells. Transport and ligand binding were characterized at different pH values using filter assays. The ACh binding site is shown to exhibit high or low affinity (K_d values are ≈10 and 200 mM, respectively). Mutation of the lysine and aspartate residues in TMDs II and IV, respectively, can decrease the fraction of sites having high affinity. In three-dimensional structures of related transporters, these TMDs lie next to each other and distantly from TMDs VIII and X, which probably contain the binding sites for ACh and the allosteric inhibitor vesamicol. Importantly, mutation of the aspartate in TMD XI can create extra-high affinities for ACh ($K_d \approx 4$ mM) and vesamicol ($K_d \approx 2$ nM compared to ≈20 nM). Effects of different external pH values on transport indicate a site that must be protonated (apparent p$K_a \approx 7.6$) likely is the aspartate in TMD XI. The observations suggest a model in which the known ion pair between lysine in TMD II and aspartate in TMD XI controls the conformation or relative position of TMD XI, which in turn controls additional TMDs in the C-terminal half of VAChT. The pH effects also indicate that sites that must be unprotonated for transport (apparent p$K_a \approx 6.4$) and vesamicol binding (apparent p$K_a \approx 6.3$) remain unidentified.

Vesicular acetylcholine transporter (VAChT,[1] SLC18A3) exchanges luminal protons for cytoplasmic acetylcholine (ACh) and concentrates ACh inside synaptic vesicles. The driving force is provided by V-ATPase, which pumps protons into the vesicles (*1*, *2*). The experimentally determined, macroscopic parameters that describe ACh transport are K_M and V_{max}. The macroscopic parameter for equilibrium binding of ACh is the dissociation constant K_{ACh}. K_M and K_{ACh} describe different types of apparent affinity, so it is not surprising that K_M is 10−100-fold smaller than K_{ACh}, depending on the species of VAChT and pH (*2*). The large difference in K_M and K_{ACh} values is key to the calculation of the microscopic constants presented below.

Transport is potently inhibited by the compound (−)-*trans*-2-(4-phenylpiperidino)cyclohexanol (vesamicol), which binds with equilibrium dissociation constant K_V to an allosteric site in VAChT (*3*). Although vesamicol is a synthetic compound, characterization of its binding is useful because the binding site is tightly linked to function.

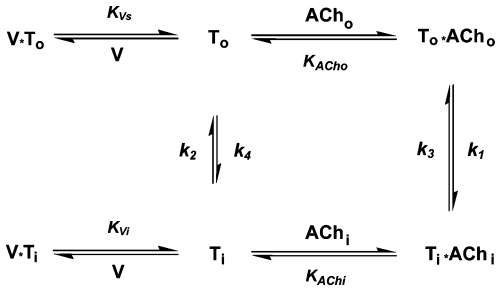

FIGURE 1: Microscopic kinetics model of the VAChT transport cycle and vesamicol (V) binding. Proton efflux is not shown.

A kinetics model for individual steps in the transport cycle is illustrated in Figure 1. Transport begins by binding of ACh on the outside, with equilibrium dissociation constant K_{AChO}, and a proton on the inside. Transmembrane reorientation then exposes bound ACh to the inside and bound proton to the outside with rate constant k_1. Both ligands are released. A second proton binds inside, after which the empty substrate binding site and bound proton reorient to the outside in the rate-limiting step k_2. The second proton is released to complete the cycle. Parameters such as K_{AChO}, k_1, and k_2 are termed microscopic because they underlie and determine the values of macroscopic parameters. Vesamicol inhibits transport by forming two types of dead-end complex, one with the substrate binding site facing outside and one facing inside (*4*).

The mathematical relationships between macroscopic and microscopic parameters for VAChT have been derived (*5*), and estimates for values of the microscopic parameters have been made (*6*). The relationships simplify to $K_{AChO} \approx K_{ACh}$,

† This research was supported by Grant NS15047 from the National Institute of Neurological Disorders and Stroke.

* To whom correspondence should be addressed. Phone: (805) 893-2252. Fax: (805) 893-4120. E-mail: parsons@chem.ucsb.edu.

[1] Abbreviations: ACh, acetylcholine; VAChT, vesicular acetylcholine transporter; vesamicol, (−)-*trans*-2-(4-phenylpiperidino)cyclohexanol; VMAT, vesicular monoamine transporter; TMD, transmembrane domain; MFS, major facilitator superfamily; K_{AChHA}, high-affinity dissociation constant for equilibrium binding of ACh; K_{AChLA}, low-affinity dissociation constant for equilibrium binding of ACh; F_{HA}, fraction of transporter having high affinity for ACh; HEPES, 2-(*N*-morpholino)ethanesulfonic acid; UBB, uptake binding buffer (110 mM potassium tartrate, 20 mM HEPES, and 1 mM ascorbic acid, pH 7.4, with KOH); paraoxon, diethyl *p*-nitrophenyl phosphate.

10.1021/bi047442y CCC: $30.25
Published on Web 05/13/2005

$k_2 \approx V_{max}/B_{max}$, and $k_1 \approx K_{ACho}k_2/K_M$. The values of microscopic K_{vs} and K_{vi} are nearly equal to each other and will be taken equal to macroscopic K_v (*5*). Thus, important microscopic parameters can be calculated from available measurements (*7*). Such an analysis is required for correct interpretation of mutational effects.

VAChT is closely related to vesicular monoamine transporter (VMAT) in physiological function, requirement for proton antiport, amino acid sequence, substrate kinetics, and existence of an inhibitory pharmacology. For this reason, observations obtained from study of VAChT and VMAT often are considered together in attempts to understand the transport mechanisms (*2*). Such aggregation will be used here as well.

VAChT and VMAT belong to the major facilitator superfamily (MFS) (*8*). Three-dimensional structures recently were obtained for three MFS transporters. The proton symporter lactose permease (*9*), the glycerol 3-phosphate phosphate antiporter (*10*), and the oxalate formate antiporter (*11*, *12*) contain the 12 helical transmembrane domains (TMDs) predicted by consensus hydropathy analysis. All three transporters have similar patterns for TMD packing consistent with conservation of supersecondary structure in the MFS.

VAChT contains 7 conserved ionic residues in 12 putative TMDs. Such residues might be involved in binding of ligands, proton translocation, or stabilization of three-dimensional conformations. They are five aspartates, a lysine, and a histidine (Figure 1). If these residues play major roles in binding and transport, those functions should depend on pH. Indeed, *Torpedo* and rat VAChT, and several isoforms and species of VMAT, all exhibit similar pH dependencies (*2*). An appropriate regression fit will yield an apparent pK_a value for each protonatable residue controlling the measured function. For VAChT and VMAT, the pH dependence of only a single mutation has been published (*13*), and a functional pK_a value has not been definitively assigned to any residue.

In important foundational work, Hersh and colleagues analyzed changes in the properties of VAChT at a single pH value after mutation of the ionic residues in TMDs (*14*, *15*). The work reported here extends that research. Major but orderly changes in the properties of mutants are revealed that provide important clues to the VAChT mechanism.

MATERIALS AND METHODS

Cell Line. The PC12$^{A123.7}$ cell line, which is derived from a line often used for study of neurosecretion, was obtained as a generous gift from L. B. Hersh (Lexington, KY). It expresses negligible endogenous VAChT (*16*). Cells were grown as described (*17*).

Mutagenesis and Transient Expression. The cDNA for wild-type rat VAChT was obtained as a generous gift from A. Roghani (Lubbock, TX). It was subcloned into the expression vector pcDNA3.1D/V5-His (Invitrogen, Carlsbad, CA) without the attached poly-His tag. Mutations were introduced, vector DNA was isolated, and cells were transfected as described (*17*). Cells were harvested after ~72 h and homogenized in 0.32 M sucrose and 10 mM HEPES adjusted to pH 7.4 with KOH [supplemented with fresh 0.1 mM phenylmethanesulfonyl fluoride (Sigma, St. Louis, MO) and complete protease inhibitor cocktail (Roche, Mannheim, Germany)]. For pH studies, the HEPES concentration was 1 mM. Homogenate was centrifuged, and postnuclear supernatant containing synaptic-like microvesicles (*18*) was quick-frozen and stored at −80 °C until used. After thawing, it was treated with 100 μM diethyl *p*-nitrophenyl phosphate (paraoxon) and assayed for protein (*19*).

Western Blot Analysis. Expression was monitored by western blot analysis as described (*20*). The primary antibody recognizes the N-terminus (Santa Cruz Biotechnology, Santa Cruz, CA).

Vacuum-Assisted Filtration. The filter assay for bound [^{3}H]-ACh or [^{3}H]vesamicol (Perkin-Elmer Life Sciences Inc., Boston, MA) has been described (*17*). Briefly, two 90 μL portions from a 200 μL incubation are mixed with separate 1 mL portions of ice-cold uptake binding buffer (UBB) composed of 110 mM potassium tartrate, 1 mM ascorbic acid, and 20 mM HEPES adjusted to pH 7.4 with KOH. The diluted portions are rapidly and quantitatively filtered, using vacuum assistance, through poly(ethylenimine)-coated glass microfiber filter circles (GF/F, 1.3 cm diameter, from Whatman, Maidstone, England) prewetted with UBB. Each filter immediately is washed with three 1 mL portions of ice-cold UBB. Radioactivity bound to the filter is determined by liquid scintillation spectrometry. Nonspecific uptake of radioligand is determined in the presence of 4 μM unlabeled vesamicol hydrochloride during incubation (except as noted). Specific uptake is the difference between total (absence of unlabeled vesamicol) and nonspecific uptake and is plotted in most of the figures.

Saturation Curves for Vesamicol Binding. [^{3}H]Vesamicol binding was determined by mixing postnuclear supernatant (100 μL) containing 100 μg of protein (unless stated otherwise) with 100 μL of UBB containing twice the indicated final concentration of [^{3}H]vesamicol. Samples were incubated for ~30 min at 23 °C. Specifically bound [^{3}H]-vesamicol was determined as described above. Appropriate equations were fitted to the averages of the duplicates by nonlinear regression to obtain the concentration of vesamicol binding sites (B_{max}) and K_v.

Equilibrium Displacement Curves for ACh. The indicated concentration of unlabeled ACh chloride was competed against a trace concentration of [^{3}H]vesamicol (5 nM, unless stated otherwise). Postnuclear supernatant (50 μL) containing 200 μg of protein (unless stated otherwise) was mixed with 100 μL of UBB containing 100 μM paraoxon and twice the indicated final concentration of unlabeled ACh. Fifty microliters of UBB containing 100 μM paraoxon and 20 nM [^{3}H]vesamicol was added, and the mixture was incubated for 10 min at 37 °C. Specifically bound [^{3}H]vesamicol was determined as described above. Appropriate equations were fitted to the averages of the duplicates by nonlinear regression to obtain high- and low-affinity dissociation constants for ACh (K_{AChHA} and K_{AChLA}).

Saturation Curves for ACh Transport. Postnuclear supernatant (50 μL) containing 200 μg of protein (unless stated otherwise) was mixed with 50 μL of UBB containing 100 μM paraoxon. Transport was initiated by the addition of 100 μL of UBB containing 100 μM paraoxon, 10 mM ATP, 4 mM $MgCl_2$, and twice the final concentration of [^{3}H]ACh. The mixture was incubated at 37 °C for 10 min before filtration. Appropriate equations were fitted to the averages

of the duplicates (normalized to B_{max} for the same preparation) by nonlinear regression to obtain maximal transport (V_{max}) and the Michaelis−Menten constant (K_M).

Immunofluorescence. Poorly transporting mutants were analyzed for proper subcellular targeting as described (*20*). Briefly, transfected cells plated onto collagen-coated glass coverslips were stained with primary goat anti-rat VAChT and rabbit anti-rat synaptophysin (Santa Cruz Biotechnology). The secondary antibodies were donkey anti-goat antibody conjugated to Cy2 dye for VAChT and donkey anti-rabbit antibody conjugated to Cy3 dye for synaptophysin. Washed coverslips were mounted in 5% *n*-propyl gallate in glycerol and viewed using a laser scanning confocal microscope (Bio-Rad Model 1024, Hercules, CA).

pH Profiles for Vesamicol Binding and ACh Transport. A buffer system of constant osmolality was developed for the pH range 5.5−10.0. A solution of 2-(*N*-morpholino)-ethanesulfonic acid/HEPES/3-[(1,1-dimethyl-2-hydroxyethyl)amino]-2-hydroxypropanesulfonic acid, each at 99.6 mM, and containing 4 mM dithiothreitol is pH 4.5 and 291 mOsm/kg. A similar solution of 2-(*N*-morpholino)ethanesulfonic acid /HEPES/3-[(1,1-dimethyl-2-hydroxyethyl)amino]-2-hydroxypropanesulfonic acid, each at 58.3 mM, and containing 4 mM dithiothreitol was adjusted to pH ∼10.5 with KOH to obtain 306 mOsm/kg. The low- and high-pH solutions were mixed with each other to obtain intermediate values (pH buffer). Use of different compounds for buffering did not change the pH profiles. Postnuclear supernatant (50 μL) containing 200−500 μg of protein in 0.33 M sucrose and 1 mM HEPES at pH 7 and 380 mOsm/kg was added to 50 μL of pH buffer. Incubation for 10 min at 37 °C for [^{3}H]ACh transport or 23 °C for [^{3}H]vesamicol binding was initiated by the addition of 100 μL of a solution containing 119 mM potassium tartrate and either (i) 10 mM ATP, 4 mM $MgCl_2$, and 2 mM [^{3}H]ACh or (ii) 10 nM [^{3}H]vesamicol (except for concentrations stated to be different). The pH of solutions i and ii was adjusted to ∼7.0 with KOH, and the pH of each incubation was measured shortly before filtration.

Statistical Analysis. Regression was performed using Scientist (MicroMath Research, St. Louis, MO) to obtain macroscopic parameters ± one standard deviation (σ). The results include calculation of a Model Selection Criterion (based on the Akaike Information Criterion), which estimates goodness of fit adjusted for the number of degrees of freedom. An experiment for each assay type was performed at least twice for each mutant (except as noted). Replicate values for fitted parameters were averaged as described (*20*).

Calculations. The k_1 value was computed for a mutant only if the value of at least one of the parameters in the calculation differed more than 3 propagated σ and a factor of 2 or more from that of wild type. Otherwise, the value of k_1 was taken as wild type even if the result of a k_1 calculation was different from that of wild type. The k_2, K_{AChHA}, and K_M values for the mutant, and not for wild type, were used in the calculation, even if the value of a parameter for a mutant was not different from that for wild type. Calculations with fully propagated estimates of errors were carried out as described (*20*).

RESULTS

The ionic residues in predicted TMDs were mutated, usually to several other amino acids, and all mutants were characterized for ligand binding and transport properties. Poorly transporting mutants also were characterized for subcellular targeting. The binding and transport data were used to calculate microscopic constants for the transport cycle. Unusual behaviors, how they were accommodated experimentally, and overall conclusions from each type of measurement are described in Results. The results then are grouped for each sequence position in the Discussion. Finally, an Overview is presented.

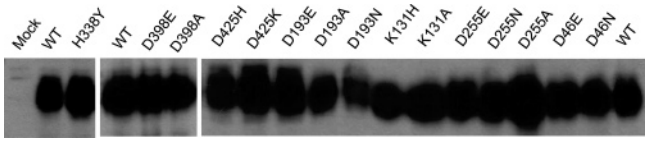

FIGURE 2: Western blots of wild-type and mutant rat VAChTs. Mock transfection did not contain the VAChT insert. VAChT runs as a diffuse band at about 85 kDa.

Western Blot Analysis. All mutants were glycosylated and not significantly proteolyzed (Figure 2). They all expressed adequately, although replicate transfections for the same mutant often gave somewhat different levels of expression.

Saturation Curves for Vesamicol Binding. Total and nonspecific binding by D398A, which gave the smallest ratio of these measurements, is shown in Figure 3A. Precision is excellent even for this worst case. Specific binding for this mutant and other interesting mutants is shown in Figure 3B. The concentrations of [^{3}H]vesamicol and VAChT were adjusted as necessary to determine very high or low affinity. Single rectangular hyperbolas fit all data sets well, which means that a single type of vesamicol binding site was present in each case (Table 2). The B_{max} values for mutants and wild type varied over ∼4-fold range, except for D398E and D398A, which had quite low values.

The very low affinities exhibited by D398E and D398A raised the possibility that much of the specifically bound [^{3}H]-vesamicol dissociated during the assay and was not detected. Accordingly, the dissociation rates at 23 °C and ice temperature were determined (data not shown). As surmised, they were fast. The result means B_{max} values obtained for D398E and D398A are large underestimates. The conclusion is confirmed by the similar intensities of staining in western blots for D398E, D398A, and wild type (Figure 2). The B_{max} problem does not extend to other mutants.

Equilibrium Displacement Curves for ACh. This type curve is determined by using unlabeled ACh to compete against a trace concentration of [^{3}H]vesamicol for binding. Trace is defined as severalfold less than K_v for the particular mutant. The procedure can yield a dissociation constant (K_{ACh}) but not a B_{max} value. After data sets for K131H and K131A were fitted with standard, hyperbolic curves, visual inspection clearly revealed that they were not well described by the fits (Figure 4A). The data are reproducible, and deviations from hyperbolic fits demonstrate that each of these displacements has at least two components, namely, high and low affinity. The components must arise from at least two forms of the ACh binding site and not two forms of the vesamicol binding site, as all [^{3}H]vesamicol saturation curves are monophasic. As justified in the Discussion for wild type, each of the data sets for K131H and K131A was fitted with the sum of two hyperbolic displacements having adjustable

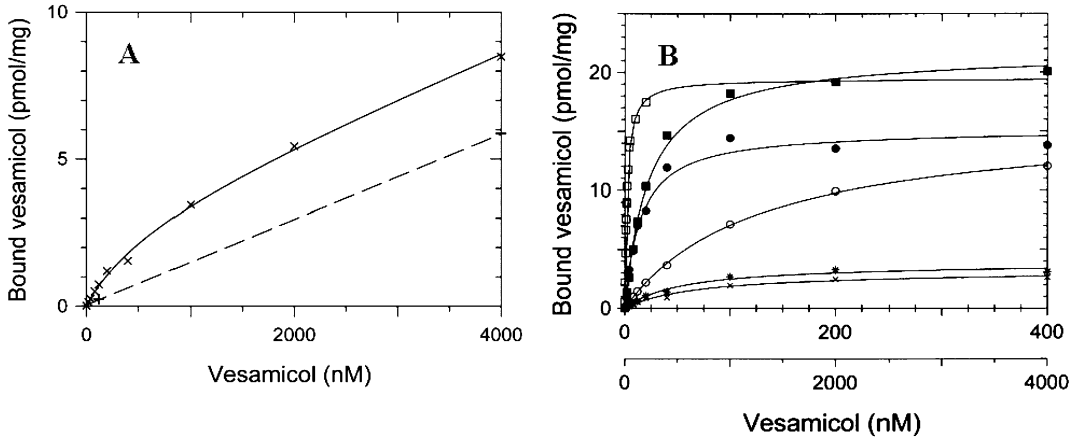

FIGURE 3: Saturation curves for [^{3}H]vesamicol binding. Frame A: Total (—) and nonspecific (– –) binding to D398A was determined in 0−4000 nM [^{3}H]vesamicol and 0−4000 nM [^{3}H]vesamicol plus 40 μM unlabeled vesamicol, respectively. At the K_v concentration, total and nonspecific binding of vesamicol corresponded to 2100 and 845 cpm, respectively, accumulated for 20 min. Frame B: Specific binding is plotted for wild-type (■) or mutant VAChT [D425K at pH 7.4 (○), D425K at pH 8.6 (●)] in 0−400 nM [^{3}H]vesamicol. Due to high affinity, D425H (□) was characterized with only 4 μg of postnuclear supernatant in 0−20 nM [^{3}H]vesamicol. Due to low affinity, D398E (∗) and D398A (×) were characterized in 0−4000 nM [^{3}H]vesamicol. Fitted parameter values for all mutants are listed in Table 2.

Table 1: Ionic Residues in TMDs of VAChT[a]

TMD[b]	I	II	IV	VI	VIII	X	XI
rat AA no.[c]	**D46**	**K131**	**D193**	**D255**	**H338**	**D398**	**D425**
rVAChT[d]	L**D**N	S**K**A	A**D**T	F**D**A	P**H**V	V**D**T	A**D**I
rVMAT1[e]	LDN	SKA	SSV	LDG	AYL	VDS	ADV
rVMAT2[e]	LDN	SKA	SSV	LDG	SYL	VDS	ADV

[a] Mutated residues are in boldface. [b] Putative TMDs are numbered from the N- to C-terminus with Roman numerals. [c] Numbers for mutated residues in the rat sequence. [d] Flanking residues are in regular font. [e] Corresponding residues in rat VMAT1 and VMAT2.

relative amplitudes (eq 1). In the equation, "fraction bound vesamicol" is the fraction of specifically bound [^{3}H]vesamicol remaining in the presence of ACh, F_{HA} is the fraction of transporter having high affinity for ACh, $1 - F_{HA}$ is the fraction of transporter having low affinity, K_{AChHA} and K_{AChLA} are the high- and low-affinity dissociation constants, respectively, and the ACh concentration is given in millimolar. The two-component equation fitted each data set very well and is sufficient to describe displacement (Table 2).

$$\text{fraction bound vesamicol} = F_{HA}\left(1 - \frac{ACh}{K_{AChHA} + ACh}\right) + (1 - F_{HA})\left(1 - \frac{ACh}{K_{AChLA} + ACh}\right) \quad (1)$$

All remaining data sets were fitted with two-component equations, and the results were compared statistically to those of the one-component fits obtained by setting F_{HA} in eq 1 to 1. Preferred fits for interesting mutants are shown in Figure 4B,C, and fitted parameter values for all mutants are listed in Table 2.

Saturation Curves for ACh Transport. Total and nonspecific transport by K131A, which gave one of the smallest ratios of these measurements, is shown in Figure 5A. Precision is good even for this near-worst case. Specific transport for this mutant and other interesting mutants is shown in Figure 5B. Single rectangular hyperbolas fit all data sets well, which means that a single type of functional transport site was present in each case. To account for variation in the amount of transport due to different expression levels, transport was normalized to B_{max}. It is not necessary to normalize K_M values.

Monophasic transport means, absent a coincidence in K_M values very unlikely to occur for all mutants, that transport is due to the form of VAChT having either high or low affinity for ACh, but not to both forms. Because the differences between high and low affinities are large (often >50-fold), very little ACh is bound to the low-affinity form at the K_M concentration of ACh. It is unlikely that the low-affinity form transports significantly.

Normalization to F_{HA}. The above analysis argues that transport also should be normalized to the fraction of the ACh binding site that is high affinity, where F_{HA} is either 1 for the mutants exhibiting one-component displacement by ACh or a fraction between 0 and 1 for mutants exhibiting two-component displacement [fully normalized is $V_{max}/(B_{max}F_{HA})$, Table 3]. The calculation of microscopic parameters must be modified to be consistent. Thus, $K_{ACho} \approx K_{AChHA}$, $k_2 \approx V_{max}/(B_{max}F_{HA})$, and $k_1 \approx k_2K_{AChHA}/K_M$.

Changes in Microscopic Constants. If the value of K_{ACho}, k_2, or k_1 for a mutant was $\geq 3\sigma$ *and* ≥ 2-fold different from that of wild type, or if the value of F_{HA} was $\geq 3\sigma$ different from that of wild type, the change was considered significant and notable. For such cases, the fold change, whether increased or decreased, and the direction of change for the mutant are listed in Table 4.

Immunofluorescence. Mutants that showed little transport were analyzed for subcellular distribution by immunofluorescence (Figure 6). All such mutants showed a pattern similar to that of wild type. Thus, the failure of some mutants to transport was not due to improper trafficking.

pH-Binding Profiles for Vesamicol. The data sets for binding of trace concentrations of [^{3}H]vesamicol at different pH values approximate bell-shaped curves in all cases (Figure 7). A bell shape means that a site with a relatively acidic pK_a value, which we arbitrarily call pK_1, must be unprotonated for vesamicol binding. Also, a different site with a relatively basic pK_a value, which we arbitrarily call pK_2, must be protonated for vesamicol binding. We asked whether any

Table 2: Equilibrium Binding of Vesamicol and ACh[a]

mutant	TMD	B_{max}[b]	K_v[c]	K_{AChHA}, K_{AChLA}[d]	F_{HA}, $1 - F_{HA}$[e]
WT		18.2 ± 0.2	22.1 ± 0.8	10.8 ± 0.7	0.89 ± 0.03
				194 ± 84	0.11 ± 0.03
D46E	I	17.6 ± 0.4	12.9 ± 1.3	26.4 ± 6.3	0.74 ± 0.13
				267 ± 178	0.26 ± 0.13
D46N		20.4 ± 0.4	20.0 ± 1.2	15.3 ± 5.7	0.72 ± 0.32
				65.5 ± 54.6	0.28 ± 0.33
K131A	II	12.5 ± 0.2	19.4 ± 0.7	10.3 ± 1.5	**0.49 ± 0.02**
				542 ± 94	**0.51 ± 0.02**
K131H		11.6 ± 0.2	13.1 ± 0.9	12.5 ± 2.5	**0.29 ± 0.02**
				1116 ± 170	**0.71 ± 0.03**
D193E	IV	46.2 ± 1.2	26.5 ± 2.1	8.74 ± 4.5	**0.34 ± 0.08**
				230 ± 43	**0.76 ± 0.08**
D193A		21.1 ± 0.5	11.3 ± 0.5	**64.7 ± 4.0**	1
D193N		13.6 ± 0.2	37.6 ± 1.6	17.1 ± 0.4	1
D255E	VI	17.4 ± 0.4	17.4 ± 1.3	14.8 ± 0.5	1
D255A		32.6 ± 1.0	12.8 ± 0.64	29.2 ± 3.7[f]	1
D255N		21.9 ± 0.6	19.4 ± 1.9	9.63 ± 1.4	0.79 ± 0.10
				57.8 ± 24.4	0.21 ± 0.10
H338Y	VIII	17.7 ± 0.2	32.0 ± 1.1	9.25 ± 0.93	0.95 ± 0.03
				1310 ± 4040	0.05 ± 0.03
D398E	X	**3.20 ± 0.18**[g]	**455 ± 65**	17.9 ± 1.7[h]	1
D398A		**3.19 ± 0.23**[g]	**691 ± 140**	22.8 ± 2.5[h]	1
D425H	XI	17.8 ± 0.4	**1.69 ± 0.11**[i]	**4.15 ± 0.34**[j]	1
D425K		15.9 ± 0.3	**126 ± 6**	**256 ± 21**	1
D425K[k]		15.1 ± 0.7	14.8 ± 2.9	**107 ± 11**	1

[a] Parameter values were obtained from experiments of the sorts shown in Figures 3 and 4 at pH 7.4, except as noted. Values are given to three significant figures ± σ. Except for F_{HA}, a parameter value at least 3 propagated σ from that of wild type *and* 2-fold different is in boldface. For F_{HA}, only a difference of 3 propagated σ was required. [b] Maximal specific binding of vesamicol (pmol/mg). [c] Wild type and all mutants exhibit a single dissociation constant for vesamicol (nM). [d] The dissociation constants for the statistically preferred monophasic or biphasic fit to displacement of trace [^{3}H]vesamicol by ACh (mM). For mutants with two entries, the biphasic fit was preferred. For mutants with one entry, the monophasic fit was preferred and the value is taken as K_{AChHA}. [e] The fraction of transporter with high (F_{HA}) or low ($1 - F_{HA}$) affinity for ACh. [f] Results from one determination. [g] Rapid dissociation of bound [^{3}H]vesamicol causes a large underestimate for B_{max}. [h] Obtained by displacement in 50 nM [^{3}H]vesamicol. [i] Obtained with 4 μg of postnuclear supernatant per 200 μL incubation to avoid significant depletion of free [^{3}H]vesamicol. [j] Obtained with 4 μg of postnuclear supernatant per 200 μL incubation and 1 nM [^{3}H]vesamicol to avoid excessive saturation of mutant. [k] pH 8.6.

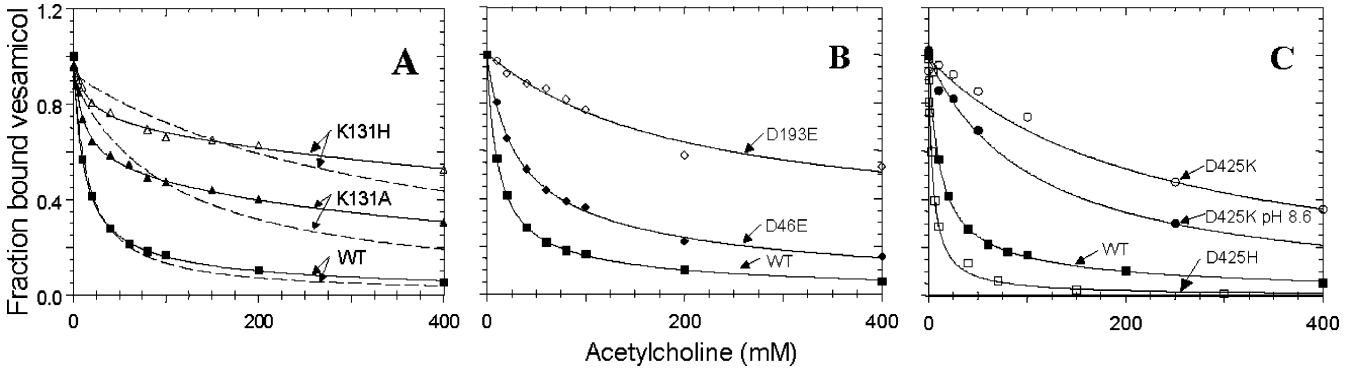

FIGURE 4: Equilibrium displacement curves for ACh. Trace [^{3}H]vesamicol was displaced by 0−400 mM nonradioactive ACh. Specifically bound [^{3}H]vesamicol is normalized to 1 at zero ACh. Frame A: Single-component (dashed line) and two-component (continuous line) fits for wild type (■), K131A (▲), and K131H (△). Frame B: The statistically preferred fit is shown for wild type (■), D46E (◆), and D193E (◇). Frame C: The preferred fit is shown for wild type (■), D425K (○), D425 at pH 8.6 (●), and D425H (□). Assay for D425H used only 1 nM [^{3}H]vesamicol and 4 μg of postnuclear supernatant. Fitted parameter values for all mutants are listed in Table 2.

of the mutations alter pK_1 or pK_2. Mutations that do so are linked structurally to the vesamicol binding site.

To estimate pK_1 and pK_2 values, each data set was fitted with eq 2, which is a standard equation for bell profiles. $B_{pHindvesamicol}$ is the "pH-independent" amount of [^{3}H]vesamicol binding to the optimally protonated state favored by intermediate pH, 10^{-pH} is the proton concentration, 10^{-pK_1} is K_1, and 10^{-pK_2} is K_2. The value of $B_{pHindvesamicol}$ is not of interest, as it depends on the concentration of vesamicol used and the K_v value for the particular mutant. Moreover, values for pK_1 and pK_2 are phenomenological and might be shifted from generic values by microenvironments, specific interactions with other residues, or a coupled equilibrium. Such shifts would not preclude recognition of an altered pH profile, but their potential presence requires that caution be exercised when interpreting a change caused by a mutation.

Fits to all of the data sets resulted in a consensus value for pK_2 of ~9.1. This value was obtained in separate experiments measuring the pK_a for the protonated amine in vesamicol (unpublished results from pH titration of the ultraviolet spectrum of vesamicol). A pK_2 event centered in vesamicol per se cannot be altered by mutation of VAChT,

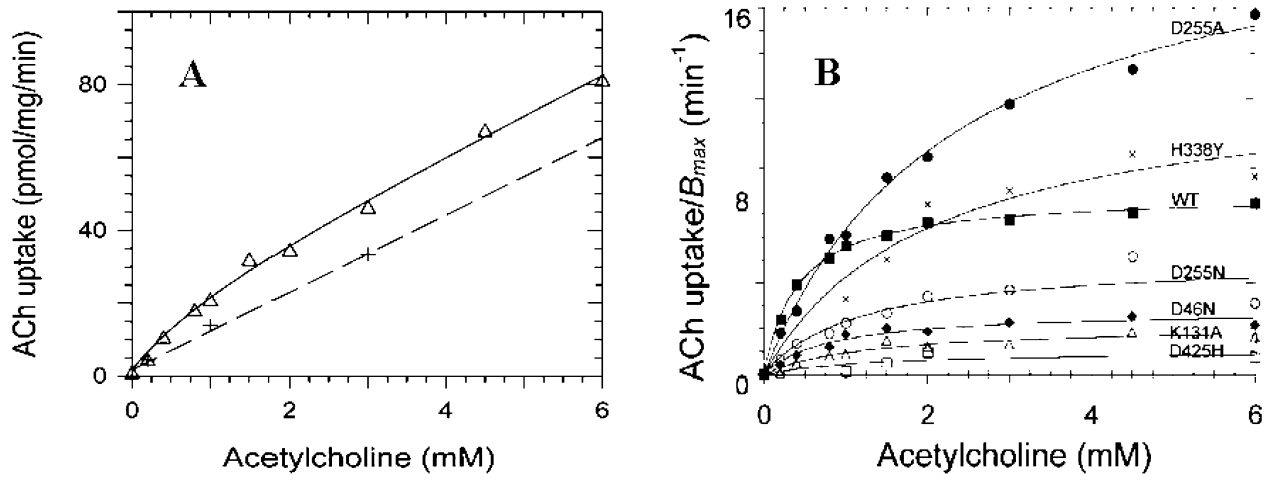

FIGURE 5: Saturation curves for [^{3}H]ACh transport. Frame A: Total (—) and nonspecific (− −) transport by K131A is shown. At the K_M concentration, total and nonspecific transport of ACh corresponded to 410 and 250 cpm, respectively, accumulated for 20 min. Frame B: Specific transport was divided by B_{max} and then plotted. Single hyperbolas representing Michaelis−Menten kinetics were fitted to data sets for wild type (■), D255A (●), H338Y (×), D255N (○), D46N (◆), K131A (△), and D425H (□). Fully normalized parameter values for all mutants are listed in Table 3.

Table 3: Macroscopic Parameters for ACh Transport[a]

mutant	$V_{max}/(B_{max}F_{HA})$[b]	K_M[c]	mutant	$V_{max}/(B_{max}F_{HA})$	K_M
WT	15.5 ± 0.9	0.77 ± 0.12	D255E	**7.05 ± 0.47**	1.67 ± 0.29
D46E	16.8 ± 3.9	0.76 ± 0.15	D255A	12.8 ± 0.64	**1.71 ± 0.19**
D46N	**5.74 ± 2.63**	2.72 ± 0.81	D255N	**7.56 ± 1.22**	1.21 ± 0.34
K131A	**4.31 ± 0.52**	1.26 ± 0.40	H338Y	8.93 ± 0.52	**1.92 ± 0.25**
K131H	20.2 ± 3.40	1.95 ± 0.69	D398E	<35.6 ± 3.3[d]	1.86 ± 0.65
D193E	21.3 ± 5.17	1.57 ± 0.25	D398A	nt[e]	nt
D193A	11.3 ± 0.5	0.91 ± 0.12	D425H	**1.55 ± 0.32**	3.90 ± 2.17
D193N	17.8 ± 0.6	0.51 ± 0.04	D425K	nt	nt

[a] Values required to compute table entries were obtained from Table 2 and experiments of the sort shown in Figure 5 at pH 7.4. Entries are given to three significant figures ± σ. An entry value at least 3 propagated σ away from that of wild type *and* 2-fold different is in boldface. [b] V_{max} normalized to the fraction of B_{max} binding ACh with high affinity ($B_{max}F_{HA}$), in units of pmol of ACh (pmol of VAChT)$^{-1}$ min^{-1}. This result is equivalent to k_2. [c] Michaelis−Menten constant in mM. [d] An overestimate due to underestimate of B_{max} caused by rapid dissociation of bound [^{3}H]vesamicol. [e] No transport was observed.

Table 4: Changes in Microscopic Parameters[a]

mutant	K_{ACho}[b]	F_{HA}[c]	$K_{vs/vi}$[d]	k_2[e]	k_1[f]	mutant	K_{ACho}	F_{HA}	$K_{vs/vi}$	k_2	k_1
D46E	WT	WT	WT	WT	WT	D255A	WT	WT	WT	WT	WT
D46N	WT	WT	WT	2.9↓	6.7↓	D255N	WT	WT	WT	2.0↓	3.6↓
K131A	WT	1.8↓	WT	3.9↓	6.2↓	H338Y	WT	WT	WT	WT	5.1↓
K131H	WT	3.1↓	WT	WT	WT	H338A[g]	nd[h]	nd	≫WT	nd	nd
D193E	WT	2.6↓	WT	WT	WT	D398E	WT	WT	21↑	nd	nd
D193A	6.0↑	WT	WT	WT	3.7↑	D398A	WT	WT	31↑	nt[i]	nt
D193N	WT	WT	WT	WT	WT	D425H	2.6↓	WT	13↓	10↓	nd
D255E	WT	WT	WT	2.2↓	3.5↓	D425K	24↑	WT	5.7↑	nt	nt
						D425K[j]	10↑	WT	4.9[k]↓	nd	nd

[a] Values for microscopic parameters were computed as described in the text for pH 7.4, except as noted. For values notably different from wild type, fold change is shown with an arrow indicating the direction of change. For example, the k_2 value for D46N was 2.9-fold smaller than for wild type. [b] Equilibrium dissociation constant for ACh binding to the outwardly oriented, high-affinity binding site. [c] Fraction of binding sites having high affinity for ACh. [d] $K_{vs/vi}$ represents K_{vs} and K_{vi} (Figure 1), which are assumed to be equal to K_v. [e] Rate determining in steady-state transport for the fraction of sites exhibiting high affinity for ACh. [f] Calculated only for mutants yielding values for $V_{max}/(B_{max}F_{HA})$ and K_M. [g] Taken from ref *15*. [h] Not determined. [i] No transport. [j] pH 8.6. [k] For protonated vesamicol (pK_2 = 9.1) binding to optimally protonated mutant and wild type using pK_1 values obtained from Table 5.

and it is not of biological interest. Thus, pK_2 in eq 2 was held at 9.1 for a final round of regression fits to obtain pK_1 values (Table 5).

$$\text{bound vesamicol} = \frac{B_{\text{pHindvesamicol}}}{1 + \dfrac{10^{-\text{pH}}}{10^{-\text{p}K_1}} + \dfrac{10^{-\text{p}K_2}}{10^{-\text{pH}}}} \qquad (2)$$

The σ estimates for many values of pK_1 in Table 5 are unrealistically small. This outcome might have occurred because (i) errors in pH were significant, possibly due to lipid fouling of the glass electrode used to measure pH, whereas errors in the independent variable are assumed to be insignificant in standard regression, and (ii) errors in pH measurements were normally distributed, which means errors in the derived proton concentrations used for the fits are log-

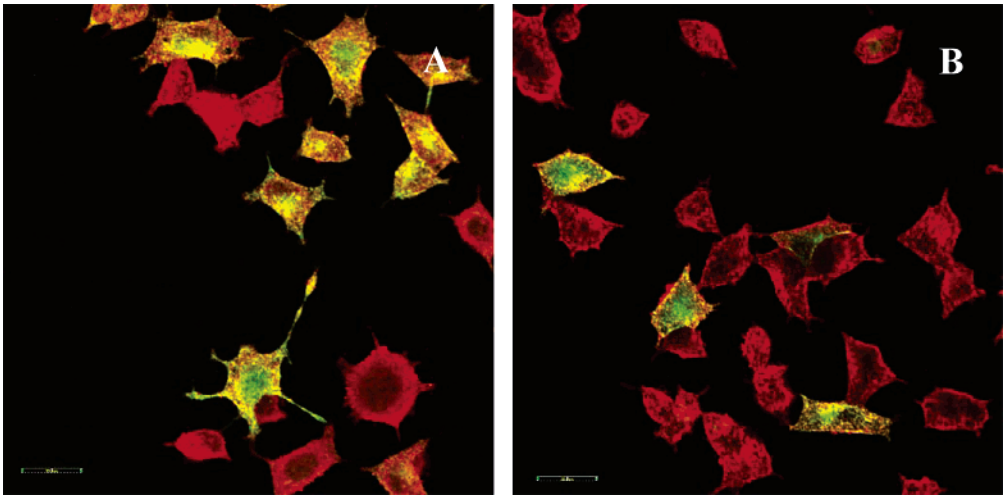

FIGURE 6: Immunofluorescent staining of VAChT and synaptophysin in synaptic-like microvesicles. PC12$^{A123.7}$ cells transiently expressing VAChT were stained green for VAChT and red for synaptophysin. Yellow indicates colocalization. Frame A is wild type. Frame B is D398A. Other mutants that transported poorly stained similarly.

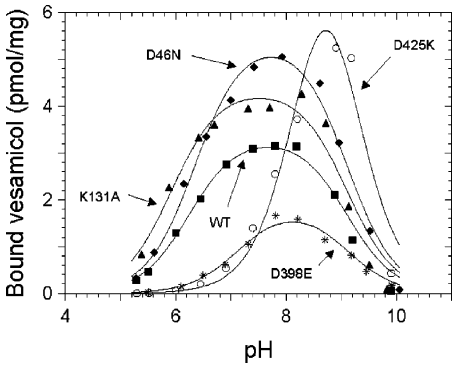

FIGURE 7: pH-binding profiles for [^{3}H]vesamicol. Bell-shaped curves were fitted to specific binding data for wild type (■), D46N (◆), K131A (▲), D398E (∗), and D425K (○). Due to low affinity, the profile for D398E was obtained in 50 nM [^{3}H]vesamicol for total binding and in 50 nM [^{3}H]vesamicol plus 40 μM unlabeled vesamicol for nonspecific binding. Fitted pK_a values for all mutants are listed in Table 5.

normally distributed (*21*). Moreover, σ does not account for a shift in apparent pK_a value due to competition between protons and the nonnegligible concentration of [^{3}H]vesamicol that was used to determine each curve. For these reasons, the threshold for a meaningful difference between values of pK_1 was increased to 1.2 units. This threshold is intuitive but representative of variability in replicate experiments, and in all cases it is greater than 3 propagated σ. Only one mutant differed from wild type by more than the threshold.

pH-Transport Profiles for ACh. The data sets for transport of nonsaturating concentrations of [^{3}H]ACh at different pH values approximate single bell-shaped curves in most cases (Figure 8A). A site with a relatively acidic pK_a value, which we arbitrarily call pK_3, must be unprotonated for transport. A different site with a relatively basic pK_a value, which we arbitrarily call pK_4, must be protonated for transport. The deprotonation and protonation requirements could occur at any step in the transport cycle, and mutations that alter pK_3 or pK_4 are structurally linked to a transport step.

To estimate values for pK_3 and pK_4, each data set approximating a bell shape was fitted with eq 3. The parameters are of the same types as those in eq 2. Similarly to pK_1, values for pK_3 and pK_4 are phenomenological and might be shifted from generic values. The threshold for a significant difference from wild type again was set at 1.2 units, and none of the differences reached the threshold (Table 5).

Table 5: pK_a Values for Vesamicol Binding and ACh Transport[a]

mutant	TMD	pK_1[b]	pK_3[c]	pK_4[d]
WT		6.28 ± 0.03	6.42 ± 0.12	7.56 ± 0.12
D46E	I	6.11 ± 0.10	6.56 ± 0.26	7.22 ± 0.28
D46N		6.36 ± 0.07	6.38 ± 0.10	8.41 ± 0.11
K131A	II	5.89 ± 0.11	6.42 (fixed at WT value)	**6.10 ± 0.20**
				9.23 ± 0.26
K131H		6.22 ± 0.12	6.29 ± 0.11	7.80 ± 0.11
D193E	IV	6.40 ± 0.11	6.15 ± 0.14	7.85 ± 0.14
D193A		7.20 ± 0.17	6.36 ± 0.13	8.12 ± 0.14
D193N		7.37 ± 0.21	6.27 ± 0.10	8.44 ± 0.10
D255E	VI	6.26 ± 0.07	6.09 ± 0.16	7.87 ± 0.20
D255A		6.36 ± 0.05	6.27 ± 0.10	8.39 ± 0.10
D255N		6.85 ± 0.08	6.20 ± 0.14	8.25 ± 0.21
H338Y	VIII	6.90 ± 0.10	6.12 ± 0.07	8.31 ± 0.08
D398E	X	7.12 ± 0.07[e]	6.68 ± 0.21	7.40 ± 0.22
D398A		7.44 ± 0.09[e]	nt[f]	nt
D425H	XI	6.30 ± 0.24	nd[g]	nd
D425K		**8.96 ± 0.10**	nt	nt

[a] Fitted values were obtained from experiments of the sorts shown in Figures 7 and 8. They are given to three significant figures ± σ. [b] The site that must be unprotonated to bind vesamicol. [c] The site that must be unprotonated to transport nonsaturating ACh. [d] The site that must be protonated to transport nonsaturating ACh. [e] Obtained in 50 nM [^{3}H]vesamicol. [f] No transport. [g] Not determined due to insufficient transport.

$$\frac{\text{ACh uptake}}{B_{max}} = \frac{v_{\text{pHindtransport}}}{1 + \frac{10^{-\text{pH}}}{10^{-\text{p}K_3}} + \frac{10^{-\text{p}K_4}}{10^{-\text{pH}}}} \quad (3)$$

K131A in TMD II exhibited a pH-transport profile composed of two overlapping bells (Figure 8B). This unusual profile is reproducible. The data were fitted by regression models that assumed (i) pK_3 and pK_4 are independently adjustable for each bell (four adjustable pK_a values), (ii) pK_3 is the same but adjustable and pK_4 is independently adjustable for each bell (three adjustable pK_a values), or (iii) pK_3 is fixed at the wild-type value and pK_4 is independently

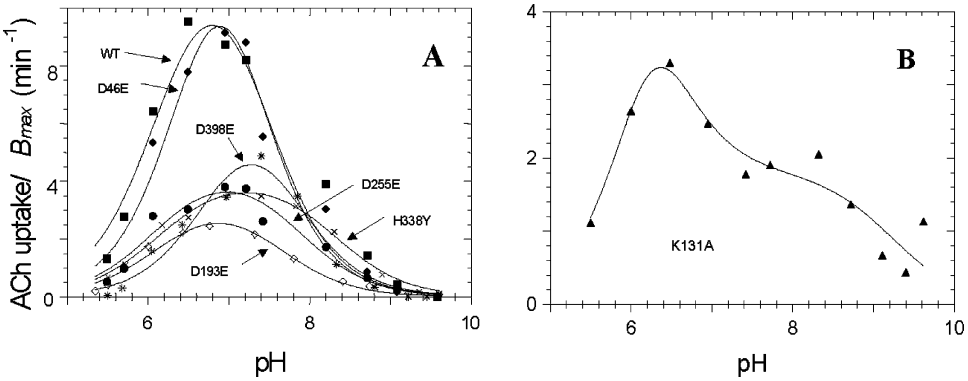

FIGURE 8: pH-transport profiles for [^{3}H]ACh. Frame A: Bell-shaped curves were fitted to specific transport data normalized to B_{max} for wild type (■), D46E (◆), D398E (∗), D255E (●), H338Y (×), and D193E (◇). Frame B: The sum of two bell-shaped curves was fitted to specific transport data normalized to B_{max} for K131A in 3 mM [^{3}H]ACh as described in the text for model iii. Fitted pK_a values for all mutants are listed in Table 5.

adjustable for each bell (two adjustable pK_a values). Model iii was preferred statistically (eq 4). The result is sensible,

$$\frac{\text{ACh uptake}}{B_{max}} = \left[\frac{v_{\text{pHindtransport1}}}{1 + \frac{10^{-\text{pH}}}{10^{-\text{p}K_3}} + \frac{10^{-\text{p}K_{4,1}}}{10^{-\text{pH}}}} + \frac{v_{\text{pHindtransport2}}}{1 + \frac{10^{-\text{pH}}}{10^{-\text{p}K_3}} + \frac{10^{-\text{p}K_{4,2}}}{10^{-\text{pH}}}}\right] \quad (4)$$

as a mutation is likely to perturb only one of the two residues responsible for the bell shape, and the profile on the acidic side resembles that of wild type. Thus, the pK_4 event was split into two events by the mutation, and the fit to the basic side gave p$K_{4,1}$ = 6.10 ± 0.20 and p$K_{4,2}$ = 9.23 ± 0.26 (Table 5). The interpretation is discussed below.

DISCUSSION

Wild Type. If data for displacement of trace [^{3}H]vesamicol by ACh are fitted with a standard hyperbolic fit, the K_{ACh} value obtained is 16.8 ± 0.7 mM. However, Ojeda et al. (*20*) found that inclusion of an adjustable Hill coefficient gives a significantly better fit consistent with apparent "negative cooperativity" of 0.75 ± 0.02. Although the Hill approach to data fitting is quantitative, it does not provide information about why a system deviates from simple behavior.

Apparent negative cooperativity can arise from (i) a homooligomer that propagates conformational changes among binding sites and (ii) a mixture of monomers having different conformations. In case i the amounts of high- and low-affinity binding must be the same, and in case ii they need not be the same. Data for K1312A, K131H, and D193E cannot be fit adequately by any reasonable variation of case i. Moreover, there is no evidence that VAChT oligomerizes. The equation describing case ii gave the preferred fit for eight of the data sets, including that of wild type, compared to the one-component fit. Thus, 89 ± 3% of wild-type VAChT has high affinity (K_{AChHA} = 10.8 ± 0.7 mM) and 11 ± 3% has low affinity (K_{AChLA} = 194 ± 84 mM) for equilibrium binding to ACh. There is no evidence in the western blots for significant proteolysis of wild type or any mutant. Intact VAChT apparently accounts for both affinity forms.

The pH studies confirm three critical types of pK_a event above pH 6 (*2*). A site with pK_1 ≈ 6.3 must be unprotonated for binding of vesamicol, a site with pK_3 ≈ 6.4 must be unprotonated for transport of ACh, and a site with pK_4 ≈ 7.6 must be protonated for transport of ACh. The pK_1 and pK_3 events could be either (i) the protonated forms acting in negative functional roles or (ii) the unprotonated forms acting in positive functional roles. Similarly, the pK_4 ≈ 7.6 event could be either (i) the protonated form acting in a positive functional role or (ii) the unprotonated form acting in a negative functional role. Insufficient information is available to decide between positive and negative roles for each event. Deprotonation of the charged ammonium center in vesamicol itself apparently accounts for loss of vesamicol binding at higher pH.

The site exhibiting pK_4 cannot mediate productive proton efflux, as protonation from the outside would be inhibitory to proton efflux and thus to transport, not stimulatory. It must have a structural role. Moreover, if the pK_4 event were to contribute to loss of vesamicol binding at higher pH, the binding would drop toward 0 twice as steeply as it does. Thus, pK_4 seen in transport has no effect on vesamicol binding.

Asp-46 in TMD I. Neither D46N nor D46E affects the fraction of VAChT that binds ACh with high affinity or the affinities of the ACh and vesamicol binding sites. D46E exhibits wild-type transport properties. D46N transports with ~3-fold lower $V_{max}/(B_{max}F_{HA})$ but wild-type K_M. These macroscopic parameters reflect 6.7- and 2.9-fold lower values for k_1 and k_2, respectively. D46 does not account for any of the pK_a events, and it is not at the ACh or vesamicol binding site.

Lys-131 in TMD II. In both VAChT and VMAT, this residue forms an ion pair with D in TMD XI (*15*, *23*). Computer modeling has confirmed that these K and D residues can be close to each other (*24*). In the current study, K131A and K131H had wild-type affinity for vesamicol. However, in K131A only 49 ± 2% has high affinity for ACh (K_{AChHA} = 10.3 ± 1.5 mM). In K131H only 29 ± 2% has high affinity (K_{AChHA} = 12.5 ± 2.5 mM). Because it behaves similarly to K131A, the mutant K131H probably does not ion pair. An absence of ion pairing might occur because the imidazole group of the introduced histidine does not carry a positive charge at the pH of the measurement (pH 7.4) or cannot extend far enough to reach D in TMD XI.

The ratios of the amounts of high- to low-affinity binding in K131A and K131H are ~0.4−1, and in wild type the ratio is 8. The ratio of ratios (~11), combined with $\Delta G^\circ = -RT \ln(K_{eq})$ in which K_{eq} is set to 11, tells us that the high-affinity form is stabilized ~−1.5 kcal/mol by the K−D ion pair. Thus, the ion pair is important but not critical to high-affinity binding by ACh.

K131H exhibits wild-type values for $V_{max}/(B_{max}F_{HA})$ and K_M. K131A shows reduced but significant transport, with $V_{max}/(B_{max}F_{HA})$ ~3.6-fold less than for wild type. K_M is wild type. The changes in transport seen for K131A are due to 6.2- and 3.9-fold slower k_1 and k_2 rate steps, respectively.

Both mutants show wild-type pH-binding profiles for vesamicol. Thus, K131 does not account for the pK_1 event. K131H shows wild-type pH-transport profiles. Thus, K131 does not account for the pK_3 or pK_4 events either. However, K131A splits pK_4 into two values, namely, p$K_{4,1} \approx 6.1$ and p$K_{4,2} \approx 9.2$ (Figure 8B). A single residue in different microenvironments likely gives rise to the splitting, as the functional consequences for protonation are the same (that is, transport). Presumably both forms of transporter represented by p$K_{4,1}$ and p$K_{4,2}$ bind ACh with high affinity, or else they could not transport. We defer discussion of which residue probably gives rise to the pK_4 event.

Because intrinsic affinities for ACh and vesamicol do not change in these mutants, K131 is not at the ACh or vesamicol binding site per se. The conclusion implies that D in TMD XI also is not at the ACh or vesamicol binding site. Disruption of the K−D ion pair surely would have affected the structure of a binding site in which the D residue of that ion pair is directly involved.

Asp-193 in TMD IV. The corresponding residue in VMAT is serine (Table 1). D193N, D193E, and D193A studied here have wild-type affinity for vesamicol. D193E, but not D193A and D193N, causes a large decrease in F_{HA} to 34 ± 8%. In D193E and D193N, some or all of the binding site for ACh is high affinity. However, in D193A all of the binding site exhibits a 6.0-fold decrease in affinity. The three mutants transport similarly to wild type at the macroscopic level, but D193A exhibits microscopic compensation. The rate of the k_1 step in this mutant increases 3.7-fold, which cancels the effect of weaker ACh binding in determining the value of K_M. D193 does not account for any of the pK_a events, and it is not located at the ACh or vesamicol binding site.

Asp-255 in TMD VI. D255E, D255A, and D255N show wild-type properties for ACh and vesamicol binding. They exhibit small decreases in $V_{max}/(B_{max}F_{HA})$ and small increases in K_M values. About 2−4-fold changes in k_1 and k_2 cause the macroscopic effects. D255 does not account for any of the pK_a events, and it is not located at the ACh or vesamicol binding site.

His-338 in TMD VIII. The previous VAChT study by Hersh and colleagues demonstrated that H338A and H338K transport ACh well but bind vesamicol poorly. Because the reverse double mutant H338D/D398H exhibits good vesamicol binding, an ion pair between H338 and D398 in TMD X was hypothesized (*15*). Computer modeling has demonstrated that these residues can be close to each other (*24*). In VMAT, the corresponding position is conserved Y (Table 1). The H338Y mutant of VAChT was made in the current study, and this nano-mimic of VMAT was characterized. It binds vesamicol and ACh with wild-type properties. It transports with wild-type $V_{max}/(B_{max}F_{HA})$ and an elevated K_M that is associated with a 5.1-fold lower value for k_1. The latter observation suggests that the interaction between TMDs VIII and X might be more important to the k_1 than the k_2 step.

As H338Y cannot acquire a positive charge, yet it substitutes adequately for H338, a positive charge, and thus an ion pair, is not critical at this position. H338Y might form a hydrogen bond with D398 that substitutes for an ion pair. Alternatively, the aromaticity of H and Y side chains might be important. H338 does not account for any of the pK_a events studied here, and it is not located at the ACh or vesamicol binding site.

Asp-398 in TMD X. In both VMAT and VAChT, this residue is very important to transport, although E substitutes (*13*, *23*). The residue probably carries the k_1 proton in VMAT (*2*). In the current study, D398E and D398A were characterized. Vesamicol binds to both mutants, but with 21- and 31-fold lower affinities, respectively. Loss of the interaction with H in TMD VIII seems sufficient explanation for lower vesamicol affinity, and there is no necessity to invoke direct participation of D398 in the vesamicol binding site. D398E and D398A have wild-type affinities for ACh, demonstrating that D398 is not part of the ACh binding site either.

Consistent with most other mutations at this position, D398A does not transport. The loss of transport without change in ACh binding properties confirms that the mutation causes a specific defect in productive efflux of protons. D398E is confirmed to transport well, but the transport could not be normalized to expression level due to an unreliable value for B_{max}. Good transport demonstrates that a negative charge is required at this position, but steric requirements for that charge are low.

The pH profiles for vesamicol binding to D398E and D398A show that pK_1 is present. Thus, D398 cannot give rise to the pK_1 event. Because D398A does not transport, pK_3 and pK_4 values could not be determined. This circumstance leaves open the possibility that D398 gives rise to the pK_3 or pK_4 event.

Several arguments constrain the possibilities. In the first argument, we assume that D398 carries the k_1 proton similarly to the corresponding residue in VMAT. As we already have concluded that the residue accounting for the pK_4 event cannot be critical to productive proton efflux, D398 cannot give rise to the pK_4 event. This argument leaves open the possibility D398 accounts for the pK_3 event, but only if different residues account for the pK_1 and pK_3 events (a relationship between D398 and pK_1 was ruled out above).

The second argument is generated by the observation that D398E exhibits wild-type values for pK_3 and pK_4. The value for pK_3 is significantly higher than for the pK_a of generic D (~4.0). If it accounts for the pK_3 event, D398 resides in a microenvironment (involving interaction with H in TMD VIII) that raises its pK_a value ~2.4 units to 6.4. Because D398E apparently does not interact with H in TMD VIII (as indicated by weak vesamicol binding), it is in a different microenvironment. Yet D398E would have to undergo a similar shift in pK_a value as D398 does to generate pK_3. This outcome is unlikely. However, the argument is not rigorous because a coincidence could occur. The pH-transport profile for the corresponding E mutant in VMAT differs considerably from that observed here (*13*).

In the third argument, if their pK_a values are generic, D398 and D398E would be essentially fully unprotonated at all pH values investigated here, and they would not generate the pK_3 event. Indeed, the site binding the k_1 proton in *Torpedo* vesicles has been assigned pK_a = 4.7 (*6*). As it likely acts in the k_1 step, D398 probably is the residue responsible for the pK_a = 4.7 event. This conclusion means D398 probably did not show its pK_a in the current work.

Asp-425 in TMD XI. This residue was mutated to H and K in order to analyze the effects of potentially positively charged residues. Positive charge would repel the substituted residue away from K in TMD II and prevent formation of a compensatory interaction mimicking the K−D ion pair in wild type. The first observation is that D425H and D425K are the only mutants to strongly perturb *both* the ACh and vesamicol binding sites. The behavior contrasts with that exhibited when the ion pair is disrupted by mutation of K in TMD II, which only decreases the fraction of high-affinity ACh binding.

The second observation is that D425H binds vesamicol 13-fold *tighter* than wild type does. The direction and size of this change are notable. At the standard pH of 7.4, D425K binds vesamicol 5.7-fold looser than wild type does. At pH 8.6, D425K has K_v = 14.8 ± 2.9 nM, which is within the range of normal affinities. However, the value is misleading. Two corrections must be made to it, using an approach similar to that given by eq 2, to compute intrinsic affinity. Because only 0.76 of the vesamicol was protonated and able to bind mutant, and only 0.30 of the mutant was unprotonated and able to bind vesamicol (Figure 7), the corrected value for pH-independent K_v is 4.1 nM. The values for D425H and wild type are 1.5 and 20 nM, respectively, after making the same types of corrections. D425K unprotonated on the introduced K binds vesamicol 4.9-fold tighter than wild type does. Thus, unprotonated K and what is probably unprotonated H (so deduced because the pH profile for vesamicol binding to D425H is the same as to wild type) both yield mutants having *extra-high affinities for vesamicol*! Unprotonated K and H are rather different structurally. These observations suggest that the increases in vesamicol affinity arise from a loss of function, namely, loss of the K−D ion pair, rather than from a gain of function dependent on the introduced K and H residues.

The third observation is that, as for vesamicol binding, the D425H and D425K mutations affect ACh binding in a complex manner (Table 2). The behavior is not an artifact caused by changes in the affinity of vesamicol, which was used as the indicator, because the conditions for the displacements by ACh were adjusted to compensate. The three sets of displacement data for these mutants are fitted best by the one-component equation. That behavior means the approximate isoenergetic relationship between high- and low-affinity forms created when the ion pair is broken on the K side is overridden when it is broken on the D side. Also, D425H exhibits 2.6-fold *extra-high affinity for ACh*. D425K binds ACh with low affinity, although binding probably is tighter at higher pH, similarly to vesamicol binding.

The diversity of residue types at this position showing normal or extra-high affinity for vesamicol and ACh [including D425N and D425E (*14*)] confirms that D425 is not at the vesamicol or ACh binding site (this conclusion already had been reached from results obtained with mutants of K in TMD II). Instead, position 425 must communicate with the ligand binding sites by means of propagated conformational changes. Moreover, the *K−D ion pair apparently blocks potential extra-high affinity* for vesamicol and ACh under some circumstances.

Transport was severely compromised in both mutants. D425K did not transport. D425H had ~10-fold lower k_2. Transport by D425H is consistent with a role for D425 in structure rather than translocation of a proton, which is similar to its role in VMAT (*13*, *23*).

D425H exhibited a wild-type value for pK_1 in vesamicol binding, which means D425 does not have a role in the pK_1 event. However, D425K exhibited p$K_1 \approx 9.0$. How can such a large increase in value be explained if the responsible wild-type residue still is present? A possible answer is that the introduced lysine blocks binding, presumably by means of a propagated conformational change, at pH values where it is protonated. Thus, the mechanisms for the pK_1 events in D425K and wild type probably are different. The value of the *apparent* pK_1 event in D425K is consistent with introduced lysine, as it is only about 1 unit lower than pK_a ≈ 10 for generic lysine.

The values of pK_3 and pK_4 could not be determined for D425K, because of the absence of transport, or for D425H, because of too little transport. Nevertheless, we conclude D425 is not likely to account for the pK_3 event. Two arguments support this conclusion. In the first argument, we note that the D425H mutant presumably must undergo deprotonation by the pK_3 event to transport even a small amount. The second argument depends on the similarity in pH dependence between VMAT and VAChT. Because an uncharged, double mutant at the K−D ion pair of VMAT transports well (*23*), the pK_3 event in VMAT is unlikely to involve D in TMD XI. By analogy, the same probably is true for VAChT.

D425 likely gives rise to the pK_4 event. The splitting of pK_4 into two values by K131A (discussed under Lys-131 in TMD II) is striking and suggests that K131, although not giving rise to the pK_4 event, is strongly linked to it. Ion pairing of K131 with D425 provides a linkage mechanism. Loss of ion pairing could allow D425 sufficient conformational flexibility to distribute between microenvironments that yield different pK_a values. Hydrophobic microenvironments are consistent with (i) increased pK_a values for D425 in wild type and K131A and (ii) a decreased pK_a value for the introduced lysine in D425K.

Overview. The findings in this study generally agree with results of previous studies in VAChT and VMAT. One interesting finding not already summarized is that mutations in TMDs I, IV, and VIII differentially affect the values of the k_1 and k_2 rate constants, which suggests that different regions of the amino acid sequence control each transmembrane reorientation step in the transport cycle. Also, *none* of the investigated residues appears to be located directly in the ACh or vesamicol binding site.

Where might the ligand binding sites be? Part of the ACh binding site probably is in TMD VIII deep in the transport channel toward vesicular lumen, as mutation of conserved W331 (~2 helical turns before H338 in TMD VIII) substantially decreases ACh affinity without effect on any other microscopic parameter (*20*). Part of the vesamicol binding site probably is in TMDs VIII and X. F335A (~1

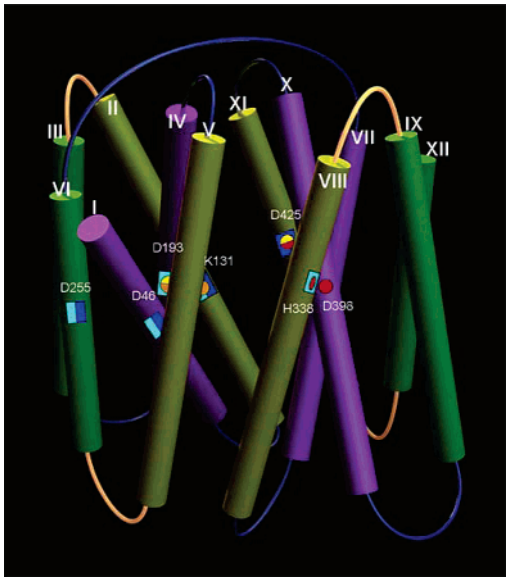

FIGURE 9: Proposed packing of TMDs in MFS transporters. The cytoplasm is on top. Residues mutated in this work are mapped very approximately into the TMDs. Effects on ligand binding are shown as circles. Vesamicol affinity is in red, ACh affinity is in yellow, and the fraction of high-affinity ACh binding is in orange. Effects on k_1 and k_2 rate constants are indicated by solid turquoise and blue rectangles, respectively. The drawing is adapted from Hirai et al. (*26*).

helical turn before H338 in TMD VIII) exhibits decreased affinity for vesamicol, and C391Y (~2 helical turns before D398 in TMD X) does not bind vesamicol, yet it transports ACh well (*20*, *25*).

All of the residues mutated in this study are definitively eliminated as the source of the p$K_1 \approx 6.3$ event in vesamicol binding. All of the residues, except those in TMDs X and XI, are definitively eliminated as the source of the p$K_3 \approx$ 6.4 event in ACh transport. Although not definitive, considerations based on the results of other work discussed above make it unlikely that the D residues in TMDs X and XI give rise to the pK_3 event. Thus, the responsible residues remain unidentified. As the pK_1 and pK_3 events (i) produce similar functional consequences, (ii) occur at nearly the same pH values, and (iii) can arise from only a few remaining candidates, a single unidentified residue of pK_a 6.3/6.4 might control both ACh transport and vesamicol binding.

All solved structures in the MFS open toward cytoplasm and show very similar TMD packing (Figure 9). Compact N- and C-terminal halves, each composed of six helical TMDs, are related to each other by a pseudo-2-fold axis perpendicular to the plane of the membrane. A putative substrate transport channel runs along the pseudo-2-fold axis. It has been argued that all members of the MFS having 12 TMDs, including VAChT and VMAT, are likely to have similar TMD packing (*24*, *26*). Accordingly, the residues mutated here have been mapped very approximately into the packing model (Figure 9). Should TMD packing in VAChT, or the locations of ligand binding sites, be shown in the future to be substantially different from those assumed here, the following discussion would have to be revised accordingly.

Mutations altering ionic residues in the putative TMDs cause orderly changes in the ligand binding and transport properties of VAChT. However, the diversity and magnitude of effects obtained by mutation of the D residue in the K−D ion pair are much greater than for any other residue. Moreover, this residue is tentatively assigned to the pK_4 event in transport. TMD XI apparently plays a special role. The observations suggest a model in which the K−D ion pair controls the conformation or relative position of TMD XI, which in turn controls additional TMDs in the C-terminal half of VAChT. The model provides an attractive explanation for how mutations in TMD IV, which lies next to TMD II, propagate consequences to the distant binding site for ACh. A mutation in TMD IV might alter the conformation of the K residue in TMD II, which could transmit the disturbance through the ion pair and into the C-terminal half of VAChT. The model also is consistent with the observation that D425E does not transport, apparently because an important structural change does not occur (*13*, *14*). These ideas suggest many new experiments to probe VAChT mechanism.

ACKNOWLEDGMENT

We thank Dr. Louis Hersh for PC12$^{A123.7}$ cells, Dr. Ali Roghani for the clone of rat VAChT, and Dr. Brian Matsumoto for assistance with confocal microscopy. We also thank Drs. Subramaniam and Hirai for providing their model of TMD packing in the MFS.

REFERENCES

1. Parsons, S. M., Prior, C., and Marshall, I. G. (1993) ACh transport, storage and release, *Int. Rev. Neurobiol. 35*, 279−390.
2. Parsons, S. M. (2000) Transport mechanisms in acetylcholine and monoamine storage, *FASEB J. 14*, 2423−2434.
3. Bahr, B. A., and Parsons, S. M. (1986). Acetylcholine transport and drug inhibition kinetics in *Torpedo* synaptic vesicles, *J. Neurochem. 46*, 1214−1218.
4. Kornreich, W. D., and Parsons, S. M. (1988) Sidedness and chemical and kinetic properties of the vesamicol receptor of cholinergic synaptic vesicles, *Biochemistry 27*, 5262−5267.
5. Bahr, B. A., Clarkson, E. D., Rogers, G. A., Noremberg, K., and Parsons, S. M. (1992) A kinetic and allosteric model for the acetylcholine transporter-vesamicol receptor in synaptic vesicles, *Biochemistry 31*, 5752−5762.
6. Nguyen, M. L., Cox, G. D., and Parsons, S. M. (1998) Kinetic parameters for the vesicular acetylcholine transporter: two protons are exchanged for one acetylcholine, *Biochemistry 37*, 13400−13410.
7. Bravo, D., and Parsons, S. M. (2002) Microscopic kinetics and structure−function analysis in the vesicular acetylcholine transporter, *Neurochem. Int. 41*, 285−289.
8. Saier, M. H., Jr., Beatty, J. T., Goffeau, A., Harley, K. T., Heijne, W. H. M., Huang, S.-C., Jack, D. L., Jahn, P. S., Lew, K., Liu, J., Pao, S. S., Paulsen, I. T., Tseng, T.-T., and Virk, P. S. (1999) The major facilitator superfamily, *J. Mol. Microbiol. Biotechnol. 1*, 257−279.
9. Abramson, J., Smirnova, I., Kasho, V., Verner, G., Kaback, H. R., and Iwata, S. (2003) Structure and mechanism of the lactose permease of *Escherichia coli*, *Science 301*, 610−615.
10. Huang, Y., Lemieux, M. J., Song, J., Auer, M., and Wang, D.-N. (2003) Structure and mechanism of the glycerol-3-phosphate transporter from *Escherichia coli*, *Science 301*, 616−620.
11. Heymann, J. A. W., Sarker, R., Hirai, T., Shi, D., Milne, J. L. S., Maloney, P. C., and Subramaniam, S. (2001) Projection structure and molecular architecture of OxlT, a bacterial membrane transporter, *EMBO J. 20*, 4408−4413.
12. Hirai, T., Heymann, J. A. W., Shi, D., Sarker, R., Maloney, P. C., and Subramaniam, S. (2002) Three-dimensional structure of a bacterial oxalate transporter, *Nat. Struct. Biol. 9*, 597−600.
13. Steiner-Mordoch, S., Shirvan, A., and Schuldiner, S. (1996) Modification of the pH profile and tetrabenazine sensitivity of rat VMAT1 by replacement of aspartate 404 with glutamate, *J. Biol. Chem. 271*, 13048−13054.

14. Kim, M.-H., Lu, M., Lim, E.-H., Chai, Y.-H., and Hersh, L. B. (1999). Mutational analysis of aspartate residues in the transmembrane regions and cytoplasmic loops of rat vesicular acetylcholine transporter, *J. Biol. Chem. 274*, 673−680.
15. Kim, M.-H., Lu, M., Kelly, M., and Hersh, L. B. (2000*)* Mutational analysis of basic residues in the rat vesicular acetylcholine transporter, *J. Biol. Chem. 275*, 6175−6180.
16. Shimojo, M., Wu, D., and Hersh, L. B. (1998) The cholinergic gene locus is coordinately regulated by protein kinase A II in PC12 cells, *J. Neurochem. 71*, 1118−1126.
17. Bravo, D. T., Kolmakova, N. G., and Parsons, S. M. (2004) Transmembrane reorientation of the substrate-binding site in vesicular acetylcholine transporter, *Biochemistry 43*, 8787−8793.
18. Weihe, E., Tao-Cheng, J.-H., Schaefer, M. K.-H., Erickson, J. D., and Eiden, L. E. (1996) Visualization of the vesicular acetylcholine transporter in cholinergic nerve terminals and its targeting to a specific population of small synaptic vesicles, *Proc. Natl. Acad. Sci. U.S.A. 93*, 3547−3552.
19. Bradford, M. M. (1976) A rapid and sensitive method for the quantitation of microgram quantities of protein utilizing the principle of protein-dye binding, *Anal. Biochem. 72*, 248−254.
20. Ojeda, A., Kolmakova, N. G., and Parsons, S. M. (2004) Acetylcholine binding site in the vesicular acetylcholine transporter, *Biochemistry 43*, 11163−11174.
21. Limpert, E., Stahel, W. A., and Abbt, M. (2001) Log-normal distributions across the sciences: keys and clues, *BioScience 51*, 341−352.
22. Merickel, A., Rosandich, P., Peter, D., and Edwards, R. H. (1995) Identification of residues involved in substrate recognition by a vesicular monoamine transporter, *J. Biol. Chem. 270*, 25798−25804.
23. Merickel, A., Kaback, H. R., and Edwards, R. H. (1997) Charged residues in transmembrane domains II and XI of a vesicular monoamine transporter form a charge pair that promotes high affinity substrate recognition, *J. Biol. Chem. 272*, 5403−5408.
24. Vardy, E., Arkin, I. T., Gottschalk, K. E., Kaback, H. R., and Schuldiner, S. (2004) Structural conservation in the major facilitator superfamily as revealed by comparative modeling, *Protein Sci. 13*, 1832−1840.
25. Zhu, H., Duerr, J. S., Varoqui, H., McManus, J. R., Rand, J. B., and Erickson, J. D. (2001) Analysis of point mutants in the *Caenorhabditis elegans* vesicular acetylcholine transporter reveals domains involved in substrate translocation, *J. Biol. Chem. 276*, 41580−41587.
26. Hirai, T., Heymann, J. A. W., Maloney, P. C., and Subramaniam, S. (2003) Structural model for 12-helix transporters belonging to the major facilitator superfamily, *J. Bacteriol. 185*, 1712−1718.

BI047442Y